Spheres and prolate and oblate ellipsoids from an analytical solution of the spontaneous-curvature fluid-membrane model

Quan-Hui Liu,[1,2,*] Zhou Haijun,[1] Ji-Xing Liu,[1] and Ou-Yang Zhong-Can[1]
[1]*Institute of Theoretical Physics, Academia Sinica, P.O. Box 2735, Beijing 100080, China*
[2]*Department of Physics, Hunan University, Changsha 410082, China*
(Received 2 March 1999)

An analytic solution for the Helfrich spontaneous curvature membrane model [H. Naito, M.Okuda, and Ou-Yang Zhong-Can, Phys. Rev. E **48**, 2304 (1993); **54**, 2816 (1996)], which has the conspicuous feature of representing a circular biconcave shape, is studied. Results show that the solution in fact describes a family of shapes, which can be classified as (i) a flat plane (trivial case), (ii) a sphere, (iii) a prolate ellipsoid, (iv) a capped cylinder, (v) an oblate ellipsoid, (vi) a circular biconcave shape, (vii) a self-intersecting inverted circular biconcave shape, and (viii) a self-intersecting nodoidlike cylinder. Among the closed shapes (ii)–(vii), a circular biconcave shape is the one with a minimum of local curvature energy. [S1063-651X(99)00309-8]

PACS number(s): 87.16.Dg, 46.70.Hg, 68.15.+e, 02.40.Hw

I. INTRODUCTION

Why red blood cells under normal physiological conditions take a circular biconcave shape (CBS) but not a spherical shape aroused the long standing curiosity of human beings since its first discovery in the 17th century. Today, physicists ascribe it to the minimization of the bending energy of a flexible lipid bilayer membrane consisting of amphiphilic molecules. The first successful model revealing the morphology was due to Canham [1] in 1970. However, his theory suffered from the shortcoming that the membrane was assumed to consist of the two identical labile surfaces, and both chemical and physical environments between the two sides of the membrane were assumed to be identical too. To overcome the shortcoming, Helfrich in 1973 introduced a phenomenological parameter, namely, the spontaneous curvature, in describing more realistic situations: the asymmetry of the two leaflets of the membrane and the chemical or/and physical differences between the interior and exterior membrane [2]. As expected, this model gave more abundant shapes than that of Canham. Based on the numerical integration technique [3], the Helfrich spontaneous curvature model yielded a catalog of axisymmetric vesicle shapes: the CBS, the prolate and oblate ellipsoid, etc. More than ten years later, the general equilibrium equation was derived by performing the variation of the Helfrich energy functional [4]. The first triumph of the equation was the prediction of the existence of a Clifford torus shaped membrane [5] and its subsequent experimental verification [6]. In 1993, a general equation in the axisymmetric case was obtained, and it is a complicated third order nonlinear differential equation [7]. An analytical solution capable of representing the CBS [8] was immediately obtained. In the same year, the first integral of the third order nonlinear differential equation was found; then the equation reduced to a second order one involving a constant of integration C [9]. An interesting fact is that an analytical solution requires a nonvanishing value of C [8,9], whereas only the special case of a second order differential equation with $C=0$ has been well studied by numerical methods [10]. In 1996, the solution was used to explain the experimentally observed polygonal shape transformation of the CBS [11]. Studies in this paper will show that this solution actually represents a family of shapes, but, in this family, CBS's have lower energies and one CBS has the lowest. For convenience, we will call this solution the CBS solution hereafter.

The existence of the analytical CBS solution in the Helfrich model proves to be remarkable, because analytical solutions to a nonlinear theory are rare and precious [12]. In very special cases of $c_0=\delta p=\lambda=0$ [cf. following Eq. (1)], the Helfrich energy functional reduces to that for constant curvature surfaces and Willmore surfaces [13], and all known analytical solutions having physical applications in membrane shapes are Delaunay surfaces, a sphere, a torus [13], and no others [14]. Therefore a systematic study of the CBS solution is necessary. We will find that there are eight types of shapes involved in the solution, and that the enclosed shapes can be grouped into prolate or oblate ellipsoid branches. These two branches are bifurcated from a sphere.

This paper is organized as follows. In Sec. II, how to obtain the CBS solution from the Helfrich model is outlined. In Sec. III, all typical shapes contained in the CBS solution are plotted and their parametrizations are presented. In Sec. IV, a systematic analysis of the CBS solution is given. In the shape family, there is a shape with a minimum energy, and in Sec. V this shape is found from the the scale invariance of the local curvature energy. In Sec. VI, a comparison of our results with previous experimental and theoretical results is given. In Sec. VII, a brief conclusion is given.

II. HELFRICH SPONTANEOUS CURVATURE MODEL AND ITS CBS SOLUTION

Equilibrium shapes of phospholipid vesicles are assumed to correspond to the minimum of the elastic energy of the closed bilayer membrane. The energy functional of the Helfrich spontaneous curvature model reads [2]

*Electronic address: liuqh@itp.ac.cn

$$F=\tfrac{1}{2}k\int (c_1+c_2-c_0)^2dA+\delta p\int dV+\lambda\int dA, \quad (1)$$

where dA and dV are the surface area and volume element for the vesicle, respectively, k is an elastic modulus, c_1 and c_2 are the two principal curvatures of the surface, and c_0 is the spontaneous curvature that describes the possible asymmetry of the bilayer membrane. When c_0 is zero, the Helfrich model reduces to the Canham model [1]. The Lagrange multipliers δp and λ take account of the constraints of constant volume and area, which can be physically understood as the osmotic pressure between the ambient and the internal environments and the surface tension, respectively. The general equilibrium shape equation is [4]

$$\delta p-2\lambda H+k(2H+c_0)(2H^2-2K-c_0H)+2k\nabla^2H=0, \quad (2)$$

where $\nabla^2=(1/\sqrt{g})\partial_i(g^{ij}\sqrt{g}\partial_j)$ is the Laplace-Beltrami operator, g is the determinant of the metric g_{ij} and $g^{ij}=(g_{ij})^{-1}$, $K=c_1c_2$ is the Gaussian curvature, and $H=-(1/2)(c_1+c_2)$ is the mean curvature. Assuming that the shape has axisymmetry, the general shape equation (2) becomes a third order nonlinear differential equation [7]

$$\begin{aligned}\cos^3\psi\left(\frac{d^3\psi}{dr^3}\right)&=4\sin\psi\cos^2\psi\left(\frac{d^2\psi}{dr^2}\right)\left(\frac{d\psi}{dr}\right)-\cos\psi\left(\sin^2\psi-\frac{1}{2}\cos^2\psi\right)\left(\frac{d\psi}{dr}\right)^3\\&+\frac{7\sin\psi\cos^2\psi}{2r}\left(\frac{d\psi}{dr}\right)^2-\frac{2\cos^3\psi}{r}\left(\frac{d^2\psi}{dr^2}\right)+\left[\frac{c_o^2}{2}-\frac{2c_o\sin\psi}{r}+\frac{\lambda}{k}-\frac{\sin^2\psi-2\cos^2\psi}{2r^2}\right]\\&\times\cos\psi\left(\frac{d\psi}{dr}\right)+\left[\frac{\delta p}{k}+\frac{\lambda\sin\psi}{kr}+\frac{c_o^2\sin\psi}{2r}-\frac{\sin^3\psi+2\sin\psi\cos^2\psi}{2r^3}\right], \quad (3)\end{aligned}$$

where r is the distance from the symmetric z axis of the rotation, and $\psi(r)$ is the angle made by the surface tangent and the r axis, as shown in Fig. 1. The positive direction of the angle is that of the angle measured clockwise from the r axis. This is contrary to the usual mathematical convention; therefore, the mean curvature H is $-\frac{1}{2}(\sin\psi/r+d\sin\psi/dr)$, in which $c_1=\sin\psi/r$ denotes the principal curvature along the parallels of the latitude, and $c_2=d\sin\psi/dr$ denotes that along those of the meridian. It is worth mentioning that the spontaneous curvature c_0 carries a sign. When the normal of a surface change its direction, c_1,c_2 and c_0 must change their signs simultaneously. Keeping the directions of r and z as usual, we have, consequently,

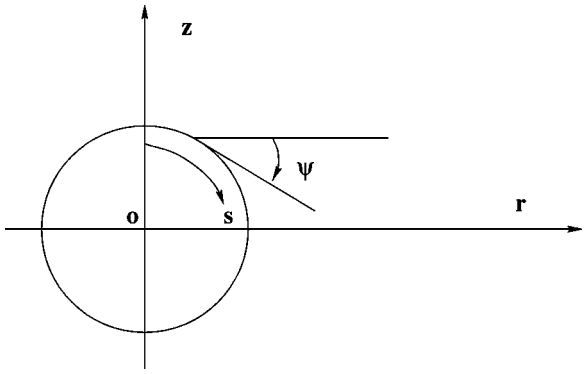

FIG. 1. Sign convention. Four arrows mean positive directions for the rotational axis z and the radial axis r, the tangent angle ψ, and the arclength s, respectively. At the north pole both the arclength s and the tangent angle ψ take zero values.

$$dz/dr=-\tan\psi(r),$$

$$z(r)-z(0)=-\int_0^r\tan\psi(r)dr, \quad (4)$$

$$\mathbf{n}=(\sin\psi\cos\phi,\sin\psi\sin\phi,\cos\psi),$$

where $\mathbf{n}$ denotes the normal of the surface and ϕ the azimuthal angle.

For self-consistency, the positive direction of the arclength s along the contour in the r-z plane must necessarilly start from the north pole of the shape. If so, we see that the parametrization for the sphere is $\sin\psi(r)=r/R_0$, where $R_0>0$ is the radius of the sphere, and our sign convention used in this paper is then compatible with that used in most previous works [3,7,10]. The third order nonlinear differential equation (3) can be simplified to be a second order one [9]

$$\begin{aligned}\cos^2\psi\frac{d^2\psi}{dr^2}-\frac{\sin(2\psi)}{4}\left(\frac{d\psi}{dr}\right)^2+\frac{\cos^2\psi}{r}\frac{d\psi}{dr}-\frac{\sin(2\psi)}{2r^2}\\-\frac{\delta pr}{2k\cos\psi}-\frac{\sin\psi}{2\cos\psi}\left(\frac{\sin\psi}{r}-c_0\right)^2-\frac{\lambda\sin\psi}{k\cos\psi}\\=\frac{C}{r\cos\psi}, \quad (5)\end{aligned}$$

where C is a constant of integration. This is still a rather complicated equation and does not belong to any known type of well-studied differential equation in mathematics.

Under the conditions that both the surface tension λ and the osmotic pressure difference δp are zero, i.e.,

$$\lambda = \delta p = 0, \tag{6}$$

an analytic CBS solution for the Eq. (3) [8,11], or Eq. (5) with $C = 2c_0$, is

$$\sin\psi = r/R_0 + c_0 r \ln r,$$

or, equivalently, (7)

$$\sin\psi = c_0 r \ln(r/r_m),$$

where R_0 is an arbitrary constant and $r_m = \exp(-1/(c_0 R_0))$. When we first obtained this solution [8,11], we concentrated on the fact that it can be used to represent the CBS of typical red blood cells [11]. In fact, by adjusting a parameter c_0 in the interval $(-\infty,\infty)$, formula (7) can give a family of shapes, which is what we are going to analyze in detail. For the sake of convenience, we mainly use the first form of the CBS solution (7) with $R_0 = 1$.

III. ALL POSSIBLE SHAPES IN THE CBS SOLUTION

Before presenting the shapes, we would like to make two comments on how to characterize them. First, for each shape, we will give both the parametrization and the interval of $r \in [0,\infty)$ in which the shape appears. This is because there may be different shapes represented by the same parametrization in distinct intervals of $r \in [0,\infty)$ as long as $|\sin\psi(r)| \leqslant 1$ is satisfied in the intervals. Second, as the scale invariance will be fully studied in Sec. V, we will follow the usual usage [10] to give, for each shape, the scale invariant $c_0 r_s$, in which $r_s = \sqrt{A/4\pi}$, with A denoting the area of the surface of the shape. Unless specifically mentioned and discussed, it is always implied that the normals of the surface point outward for closed shapes. All possible types of shapes represented by Eq. (7) are listed in the following.

(i) The flat plane (trivial case) with $c_0 r_s = 0$:

$$\sin\psi = 0, \quad r \in [0,\infty]. \tag{8}$$

(ii) The sphere with $c_0 r_s = 0$:

$$\sin\psi = r/R_0, \quad r \in [0,R_0]. \tag{9}$$

(iii) The prolate ellipsoid. A typical shape with $c_0 r_s = -0.72$ is shown in Fig. 2(a), and one of its parametrizations is

$$\sin\psi = r - 0.6 r \ln r, \quad r \in [0,1]. \tag{10}$$

Another parametrization representing the same shape is $\sin\psi = r - 1.85 r \ln r$, $r \in [0,0.324]$. The parametrization $\sin\psi = r + 4.063 r \ln r$, $r \in [0,0.148]$ represents the same shape but with an inward pointing normal.

(iv) The capped cylinder. A typical shape with $c_0 r_s = -2.06$ is shown in Fig. 2(b), and one of its parametrizations is

$$\sin\psi = r - 0.99 r \ln r, \quad r \in [0,1]. \tag{11}$$

Another parametrization representing the same shape is $\sin\psi = r - 1.01 r \ln r$, $r \in [0,0.980]$. The parametrization $\sin\psi = r + 3.5913 r \ln r$, $r \in [0,0.275]$ represents the same shape but with an inward pointing normal.

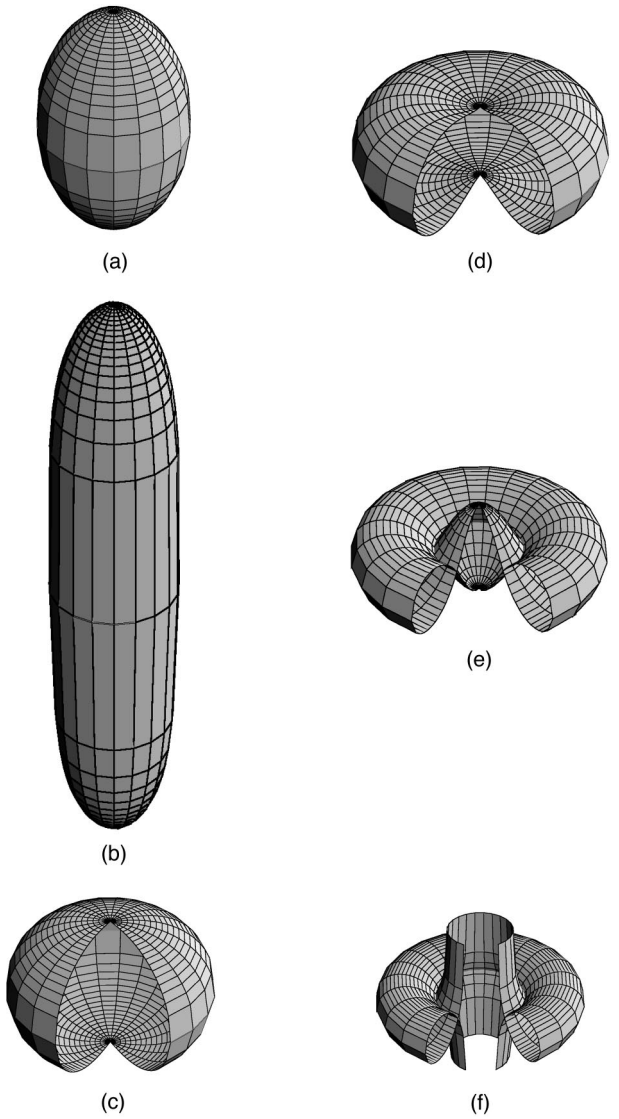

FIG. 2. The nontrivial shapes in the CBS solution: the prolate ellipsoid (a), the capped cylinder (b), the oblate ellipsoid (c), the CBS (d), the self-intersecting inverted CBS (e), and the self-intersecting nodoidlike cylinder (f).

(v) The oblate ellipsoid. A typical shape with $c_0 r_s = 0.46$ is shown in Fig. 2(c) and its parametrization is

$$\sin\psi = r + 0.5 r \ln r, \quad r \in [0,1]. \tag{12}$$

(vi) The CBS. A typical shape with $c_0 r_s = 1.51$ is shown in Fig. 2(d), and its parametrization is

$$\sin\psi = r + 1.8 r \ln r, \quad r \in [0,1]. \tag{13}$$

(vii) The self-intersecting inverted CBS. A typical shape with $c_0 r_s = 2.72$ is shown in Fig. 2(e), and its parametrization is

$$\sin\psi = r + 3.2 r \ln r, \quad r \in [0,1]. \tag{14}$$

We note that, in this case, the outside of this shape can be defined but we cannot let the normal always point outward

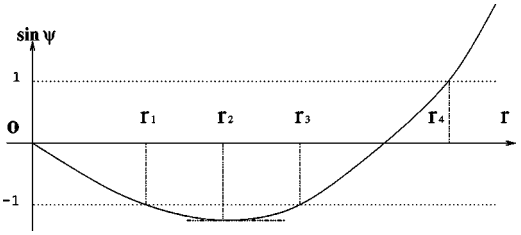

FIG. 3. The relation of $\sin\psi(r)$ vs r and the intervals where the shapes appear. When $0<c_0<c_r$ and $-1<\sin\psi(r_2)<0$, shapes appear in $[0,r_4]$. When $c_0\geqslant c_r$ and $\sin\psi(r_2)\leqslant -1$, shapes appear in two distinct intervals $[0,r_1]$ and $[r_3,r_4]$.

using a single parametrization [Eq. (14)]. The normal of the parametrization [Eq. (14)] points outward only at the surface of the torus part.

(viii) The self-intersecting nodoidlike cylinder. This situation was discussed in a previous paper [12]. We add a typical figure [Fig. 2(f)] in this paper for completeness. The cylinder is infinitely long with periodic packing, along the rotational axis, of a basic unit in which self-intersecting occurs once. We plot the basic unit only. We use the surface of the basic unit to calculate r_s, and the shape has $c_0 r_s = 3.28$. Its parametrization is

$$\sin\psi = r + 3.60 r \ln r, \quad r \in [0.301,1]. \tag{15}$$

The normal of this parametrization also points outward only at the surface of the torus part also. We note that the same parametrization $\sin\psi = r + 3.60 r \ln r$ in interval $r \in [0,0.257]$ gives a capped cylinder, but that its normal points inward.

These eight shapes consist of all possible types of shapes contained in the solution. From the parametrizations of the these shapes, one may note two facts that the spontaneous curvatures of all shapes are within a very narrow domain instead of an infinite domain of $c_0 \in (-\infty,\infty)$, and that a single shape may have different parametrizations. Explanations of these facts will be given in Sec. IV by both qualitative and quantitative studies of the CBS solution.

IV. QUANTITATIVE STUDY OF SHAPES IN THE CBS SOLUTION

All the closed shapes (ii)–(vii) presented in Sec. III can be grouped into two branches: A prolate ellipsoid branch including (ii)–(iv) shapes, and an oblate ellipsoid branch including (ii) and (v)–(vii) shapes; these two branches are bifurcated from a sphere (ii). This is easily understandable if looking into the CBS solution (7) $\sin\psi = r/R_0 + c_0 r \ln r$. When $R_0 > 0$ and $c_0 = 0$, this form gives nothing but a sphere of radius R_0. Then, when c_0 is a small quantity, positive c_0 leads to an oblate ellipsoid and negative c_0 leads to a prolate ellipsoid, respectively. The case when c_0 is large is not so evident, and needs some reasoning.

To analyze how c_0 affects the shapes and the intervals of r such that $|\sin\psi(r)| \leqslant 1$, we use the parametrization $\sin\psi = r + c_0 r \ln r$, and sketch the relation of $\sin\psi$ with positive c_0 vs r in Fig. 3. From this figure, we see that $\sin\psi = r + c_0 r \ln r$ is a single-valued and monotonous function of r; it reaches its extremum at point r_2, which satisfies

$$\frac{d\sin\psi}{dr} = 1 + c_0 + c_0 \ln r_2 = 0, i.e., r_2 = \exp\left(-\frac{1+c_0}{c_0}\right). \tag{16}$$

The extremum value of $\sin\psi(r_2)$ is

$$\sin\psi(r_2) = -r_2 c_0 = -c_0 \exp\left(-\frac{1+c_0}{c_0}\right), \tag{17}$$

which is negative for positive c_0, and vice verse. Taking positive c_0 as an example in Fig. 3, corresponding to different c_0's, shapes can appear in different intervals of r. There are three different cases of $c_0 \in [0,\infty)$. (i) When c_0 is critical such that $\sin\psi(r_2) = -1$, we have $c_0 = c_r \approx 3.591\,12$ from Eq. (17). The meridian principal curvature vanishes at point r_2 as $c_2 = d\sin\psi/dr = 0$: it is the unphysically infinitely long capped cylinder with radius $r_2 = 1/c_0 = 0.278$ from Eq. (17). (ii) When $c_0 < c_r$, we have $\sin\psi(r_2) > -1$ and shapes appear in one interval $[0,r_4]$ in which r_4 are the equatorial radii of the shapes such that $\sin\psi(r_4) = 1$. Along the increase of r from 0 to r_4, the tangent angle $\psi(r)$ decreases from zero and reaches its minimum at point r_2, then increases monotonously and reaches its maximum value $\psi = \pi/2$ at point r_4. These shapes certainly belong to the oblate ellipsoid branch, and their normals point outward from Eq. (4). (iii) When $c_0 > c_r$, we have $\sin\psi(r_2) < -1$, and shapes can appear in two distinct intervals $[0,r_1]$ (with r_1 being the equatorial radii of the shapes such that $\sin\psi(r_1) = -1$) and $[r_3,r_4]$, because in both intervals $|\sin\psi(r)| \leqslant 1$ is satisfied. In interval $[0,r_1]$, the tangent angle $\psi(r)$ decreases from zero and terminates at $\psi(r_1) = -\pi/2$. These shapes certainly belong to the prolate ellipsoid branch, but the normals point inward since $-1 \leqslant \sin\psi(r) \leqslant 0$ holds for the whole interval $r \in [0,r_1]$. In a distinct interval $[r_3,r_4]$, numerical studies show that only the self-intersection nodoidlike cylinder appears.

In fact, using the parametrization $\sin\psi = r/R_0 + c_0 r \ln r$, each shape with a c_0 outside the domain $(-1,c_r)$ can be found be identical, with a value of c_0 within the domain $(-1,c_r)$. To demonstrate this fact, we resort to the second form of the CBS solution $\sin\psi = c_0 r \ln(r/r_m)$ in Eq. (7). Two parametrizations $c_0 r \ln(r/r_m)$ and $-c_0 r \ln(r/r_m)$ represent the same shape, but the normal of one is opposite that of the other's from Eq. (4). If we require that the normal points outward, one of these two parametrizations must be eliminated. Furthermore we have a simplified form

$$\sin\psi = c_0 r \ln(r/r_m) = (c_0 r_m)(r/r_m)\ln(r/r_m) = c_0' x \ln x \tag{18}$$

where $x = r/r_m$ is the dimensionless length, and $c_0' = c_0 r_m = c_0 \exp(-1/(c_0 R_0))$ is a dimensionless spontaneous curvature. One can find that c_0' in two separate domains $c_0' \in (-\infty,-e)$ and $c_0' \in [0,e)$, in which e is the base of the natural logarithm, suffice to give all possible shapes with normals pointing outward in the CBS solution. When $c_0' = \pm e$, the shapes are unphysically infinitely long capped cylinders. From the relation $c_0' = c_0 \exp(-1/(c_0 R_0))$, and letting $R_0 = 1$, all shapes can be mapped into a single domain $c_0 \in (-1,c_r)$ in parametrization $\sin\psi = r/R_0 + c_0 r \ln r$. This is why only a few shapes of spontaneous curvature c_0 within a

narrow domain in Sec. III are sufficient to give all possible types of shapes in the CBS solution, i.e., why each shape with a c_0 outside the domain $(-1,c_r)$ can be found to be identical, with a value of c_0 within the domain $(-1,c_r)$.

In addition to the above qualitative analyses, a numerical method will be used to characterize the shapes in the whole domain $c_0 \in (-\infty,\infty)$ quantitatively. We introduce two ratios, a semiaxis ratio $z(r_0)/r_0$ and a reduced radius ratio r_v/r_s. The so-called semiaxis ratio $z(r_0)$ is defined by half of the distance of two poles of a vesicle in the symmetrical axis z, which is

$$z(r_0)-z(0)=-\int_0^{r_0}\tan\psi(r)dr, \tag{19}$$

where r_0 is the equatorial radius of the vesicle satisfying $\sin\psi(r_0)=\pm 1$. The ratios $z(r_0)/r_0$ are plotted by dashed lines in Fig. 4. In Fig. 4(b), c_0 approaches -1 and c_r, and the ratio $z(r_0)/r_0$ approaches infinity: the shapes are infinitely long capped cylinders with radii of 1 and 0.278, respectively. When c_0 increases from -1 to c_r, the ratio decreases monotonically. In sequence we have a capped cylinder, a prolate ellipsoid and a sphere of unit radius at $c_0=0$, an oblate ellipsoid with a small positive c_0, a CBS whose center touches at $c_0=2.4288$, and a self-intersecting inverted CBS. From Figs. 4(a) and 4(c), we clearly see that when $c_0<-1$ or $c_0>c_r$, the ratios $z(r_0)/r_0$ are greater than 1. In sequence we have a capped cylinder, a prolate ellipsoid, and a quasisphere with increasing $|c_0|$. When $|c_0|$ approaches infinity, the constraint $|\sin\psi(r)|\leqslant 1$ means that r_1 (cf. Fig. 3), must be very small. Thus we have approximately $\sin\psi(r)\simeq\mp c_0 r$ for positive and negative c_0's, respectively, using the L' Hospital method. This implys that we will again have a sphere. All these shapes are closed, and appear in intervals of r including the point $r=0$, which are physically interesting and are plotted in Fig. 4. When $c_0<-1$ or $c_0>c_r$, in intervals $[r_3>0,r_4]$ (cf. Fig. 3), we have self-intersecting nodoidlike cylinders, which are less physically interesting and which have not been plotted in Fig. 4. As pointed out in Ref. [12], along with the increasing $|c_0|$, the number of self-intersections the in unit length increases, and the unit length approaches a quasitorus as $|c_0|$ approaches ∞. In fact, when $-1<c_0\leqslant 0$, self-intersecting nodoidlike structures also appear in the intervals $[r_3>0,r_4]$, but, along with the decreasing $|c_0|$, the number of self-intersections in the unit length increases.

The second ratio is r_v/r_s, in which r_v is defined by the radius of a sphere having the same volume V as a vesicle, and r_s by the radius of a sphere having the same area A as a vesicle. The volume V and area A are

$$V=4\pi\int_0^{r_0}\frac{r(z(r)-z(0))}{\cos\psi}dr, \tag{20}$$

$$A=4\pi\int_0^{r_0}\frac{r}{\cos\psi}dr. \tag{21}$$

Undoubtedly, we have $r_v/r_s\leqslant 1$, and the equality holds for the sphere only. The ratio is plotted by dot-dashed lines in Fig. 4.

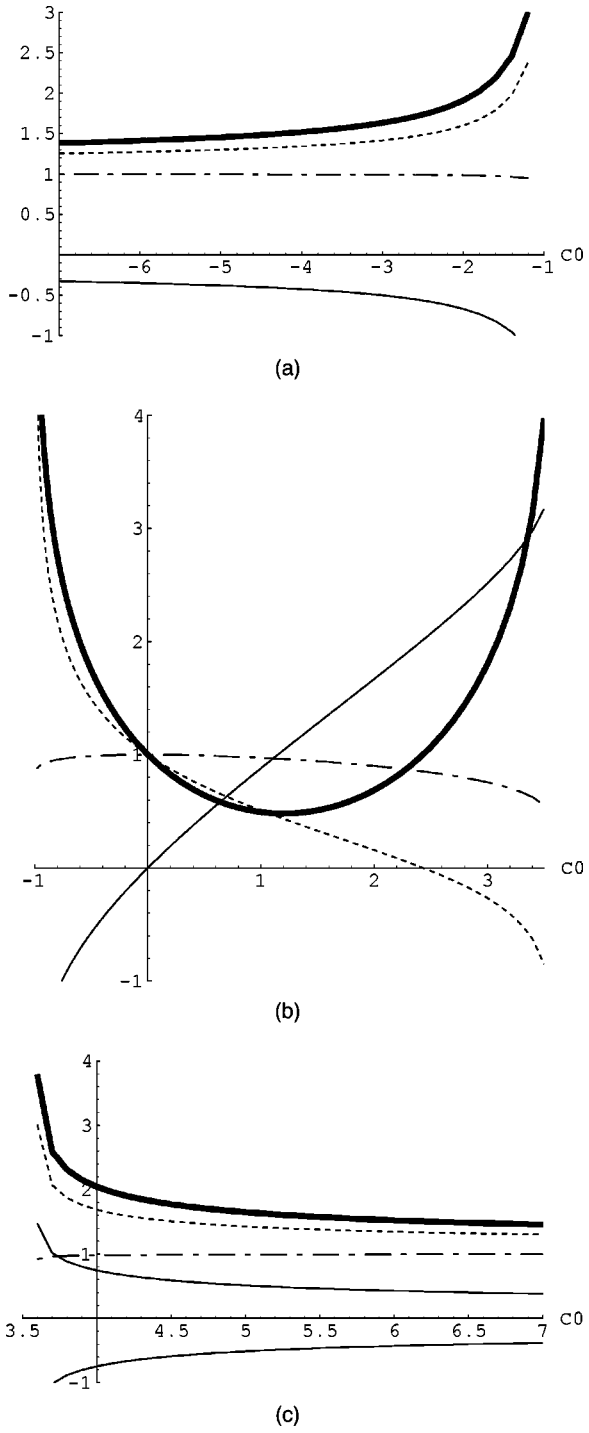

FIG. 4. The energy (thick solid line), the scale invariant $c_0 r_s$ (thin solid line), and two ratios $z(r_0)/r_0$ (dashed line) and r_v/r_s (dot-dashed line), in three domains $-7\leqslant c_0\leqslant -1.2$ (a), $-0.98\leqslant c_0\leqslant 3.5$ (b), and $3.6\leqslant c_0\leqslant 7$ (c) for closed shapes. The bending elastic modulus k used to scale the energy of a sphere to unit. All quantities in four curves are dimensionless. In order to see clearly the fact that a shape with an exclusive value of $c_0\in(-\infty,-1)$ and a shape with an exclusive value of $c_0\in(c_r,\infty)$ are identical except that the normals point inward and outward, respectively, in the last figure (c) we plot both $c_0 r_s$ (above the c_0 axis) and $-c_0 r_s$ (below the c_0 axis) by the same thin solid lines. We can also see that all shapes with $c_0\in(-\infty,-1)$ and $c_0\in(c_r,\infty)$ have corresponding identical the shapes with $c_0\in(-1,0)$. A single domain $c_0\in(-1,c_r)$ thus suffices to give all the shapes.

The scale invariant $c_0 r_s$ is plotted by thin solid lines in Fig. 4. In Fig. 4(c), we plot both $c_0 r_s$ (above the c_0 axis) and $-c_0 r_s$ (below the c_0 axis) by the same thin solid lines, in order to see the fact that each shape with a $c_0 \in (-\infty, -1)$ is identical to a shape with a $c_0 \in (c_r, \infty)$, and vice versa. However, the normals of shapes parametrized by $\sin\psi = r + c_0 r \ln r$ with $c_0 \in (c_r, \infty)$ point inward. From both qualitative and quantitative studies in this section, we can draw the conclusion that all possible closed shapes in the CBS solution (8) are, along with c_0 increasing from -1 to c_r, a capped cylinder, a prolate ellipsoid, a sphere, an oblate ellipsoid, a CBS, and a self-intersecting inverted CBS.

V. SCALE INVARIANCE OF THE ENERGY AND THE SHAPE WITH MINIMUM ENERGY

An important property of the local curvature energy is its scale invariance. This energy does not depend on the size of the vesicle but only on its shape [10]. If **R** is a solution with a local curvature energy, the rescaled shape $\mathbf{R} \rightarrow \mathbf{R}/k$ with $k>0$, and consequently $(c_1, c_2, c_0, dA) \rightarrow (kc_1, kc_2, kc_0, dA/k^2)$, is also a solution with the same local curvature energy. Two parametrizations of the CBS solution (8) having manifest scale invariance are

$$\sin\psi(r) = r/R_0 + c_0 r \ln(r/r_0) \quad \text{and}$$

$$\sin\psi(r) = c_0 r \ln(r/r_0), \tag{22}$$

in which r_0 is a constant with length unit as r or R_0. It is evident that the two products $c_0 r_s$ and $c_0 r_v$ are two scale invariants independent of a particularly chosen parametrization. We used two particular parametrizations, $\sin\psi(r) = r/R_0 + c_0 r \ln r$ and $\sin\psi(r) = c_0 r \ln r$, to search for the minimum energy shape. Both give the same results $c_0 r_s = 1.04$ and $c_0 r_v = 1.00$. The minimum energy is 0.480; hereafter we take the energy of the sphere, $8\pi k$, as the energy unit. Surprisingly, the CBS with a center touching at $c_0 = 2.4288$ has an energy 1.00. In Fig. 4(b), the thick solid line shows that there is an energy minimum shape with $c_0 = 1.200$: it is a CBS. In general, oblate ellipsoids including the CBS have a lower energy than other shapes, including the sphere, the prolate ellipsoid, and the self-intersecting inverted CBS.

VI. COMPARISON OF OUR RESULTS WITH THE PREVIOUS EXPERIMENTAL AND THEORETICAL RESULTS

All previous numerical studies concentrated on the solution of the equation when $C=0$ of Eq. (5), and the obtained shapes [10,16] included all eight shapes mentioned above. All these eight shapes except the self-intersecting cases have been observed in the laboratory [15–17].

Since our solution belongs to the situation $C \neq 0$ of Eq. (5), our results coincide with the known theoretical results in one respect, but differ from in another. First, our approach supports the conclusion that prolate ellipsoids may have a higher energy than the oblate ones have [4]. However, the standard instability analysis of a sphere starts from a slightly deformed sphere of parametrized form $r = R_0 + \Sigma a_{lm} Y_{lm}(\theta, \phi)$, where a_{lm} is a set of small parameters corresponding to spherical harmonics $Y_{lm}(\theta, \phi)$. For small a_{lm}, for example, the only nonvanishing $a_{2,0}$ satisfying $|a_{2,0}| \ll R_0/2$, the ellipsoids have C^∞ contour curves. But our ellipsoids have only C^1 contour curves, We must stress that the C^1 continuity suffices to ensure that the membranes are free from any force acting on any point. The second derivative of $z(r)$ with respect to r is singular at point $r=0$. One may feel uneasy about this singularity. In fact, it relates to energy density only, and the total energies $(1/2)k\int(c_1 + c_2 - c_0)^2 dA$ are limited, as shown in Fig. 4. Second, the infinitely long capped cylinders appear when $c_0 = -1$ and $c_0 = c_r$, and they correspond to infinite energy states, as shown by thick solid lines in Figs. 4(a)–4(c). From our results, the phases between the two sides of $c_0 = -1$ and $c_0 = c_r$ are separate. The latter c_r distinguishes an oblate ellipsoid phase and a prolate ellipsoid phase; this is the same situation as in the known phase diagram [10]. However when c_0 changes from $c_0 < c_r$ to $c_0 > c_r$, the normal changes its direction from outward pointing to inward pointing. It seems that the membrane takes a global flip-flop procedure. However, no such procedure takes place when c_0 changes from $c_0 < -1$ to $c_0 > -1$, even when the transitions are also discontinuous. Third, an interesting number appeared both in our results and the previous ones: $c_0 R_0 = 1.200$. We see from Fig. 4(b) that when $c_0 R_0 = 1.200$, where $R_0 = 1$ in our parametrization, the CBS has the minimum energy. In the usual instability analysis of a sphere via an infinitesimal deformation, the infinitesimally deformed oblate shape has a lower energy and is more stable than the infinitesimally deformed prolate one whenever $c_0 R_0 < -1.2$ [4].

VII. CONCLUSION

An analytical solution for the Helfrich spontaneous curvature membrane model [8,11], which has a conspicuous feature of representing the circular biconcave shape, is systematically studied in this paper. Results show that the solution in fact describes a family of shapes, which can be classified as (i) a flat plane (trivial case), (ii) a sphere, (iii) a prolate ellipsoid [Fig. 2(a)], (iv) a capped cylinder [Fig. 2(b)], (v) an oblate ellipsoid [Fig. 2(c)], (vi) a CBS [Fig. 2(d)], (vii) a self-intersecting inverted CBS [Fig. 2(e)], and (viii) a self-intersecting nodoidlike cylinder [Fig. 2(f)]. All these shapes have been found in numerical solutions of Eq. (5) with $C=0$ [9]. Except for self-intersecting cases, they all have real correspondence *in vitro* and *in vivo* on vesicle shapes [15–17]. The closed shapes (ii)–(vii) form two separate prolate and oblate ellipsoid branches which are bifurcated from a sphere. The oblate ellipsoids including the CBS have a lower energy than the prolate ellipsoids including the sphere, and a CBS with $c_0 r_v = 1.00$ has the lowest energy. The usual instability analysis of a sphere leads to the conclusion that the least stable shapes are prolate and oblate ellipsoid branches [4,18], but to our knowledge this is the first time an explicit parametrization has been given to show how these two branches come out gradually and analytically.

ACKNOWLEDGMENTS

We are indebted to Professor Zheng Wei-Mou for enlightening discussions. This work is supported by the National Natural Science Foundation of China.

[1] P.B. Canham, J. Theor. Biol. **26**, 61 (1970).
[2] W. Helfrich, Z. Naturforsch. C **28c**, 693 (1973).
[3] H. J. Deuling and W. Helfrich, Biophys. J. **16**, 861 (1976); J. Phys. (France) **37**, 1335 (1976).
[4] Ou-Yang Zhong-Can and W. Helfrich, Phys. Rev. Lett. **59**, 2486 (1987); Phys. Rev. A **39**, 5280 (1989).
[5] Ou-Yang Zhong-Can, Phys. Rev. A **41**, 4517 (1990).
[6] M. Mutz and D. Bensimon, Phys. Rev. A **43**, 4525 (1991).
[7] Hu Jian-Guo and Ou-Yang Zhong-Can, Phys. Rev. E **47**, 461 (1993).
[8] H. Naito, M. Okuda, and Ou-Yang Zhong-Can, Phys. Rev. E **48**, 2304 (1993).
[9] W. M. Zheng and J. X. Liu, Phys. Rev. E **48**, 2856 (1993).
[10] U. Seifert, K. Berndl, and R. Lipowsky, Phys. Rev. **44**, 1182 (1991); U. Seifert, Adv. Phys. **46**, 13 (1997); U. Seifert and R. Lipowsky, in *Handbook of Biological Physics*, edited by R. Lipowsky and E. Sackman (Elsevier, Amsterdam, 1995).
[11] H. Naito, M. Okuda, and Ou-Yang Zhong-Can, Phys. Rev. E **54**, 2816 (1996).
[12] H. Naito, M. Okuda, and Ou-Yang Zhong-Can, Phys. Rev. Lett. **74**, 4345 (1995).
[13] J. C. Nitsche, *Lectures on Minimal Surfaces* (Cambridge University Press, Cambridge, 1989), Vol. 1.
[14] A. I. Bobenko, Math. Ann. **290**, 209 (1991); U. Pinkall and I. Sterling, Math. Intell. **9**, 38 (1987).
[15] H.-H. Dobereiner, E. Evans, M. Krauss, U. Seifert, and M. Wortis, Phys. Rev. E **55**, 4458 (1997).
[16] T. Umeda, H. Nakajima, and H. Hotani, J. Phys. Soc. Jpn. **67**, 682 (1998).
[17] M. Bessis, *Living Blood Cells and their Ultrastructure*, translated by R. I. Weed) (Springer-Verlag, Berlin, 1973); *Red Cell Shape (Physiology, Pathology, Ultrastructure)* (Springer-Verlag, Berlin, 1973).
[18] M. A. Peterson, Phys. Rev. A **39**, 2643 (1989).